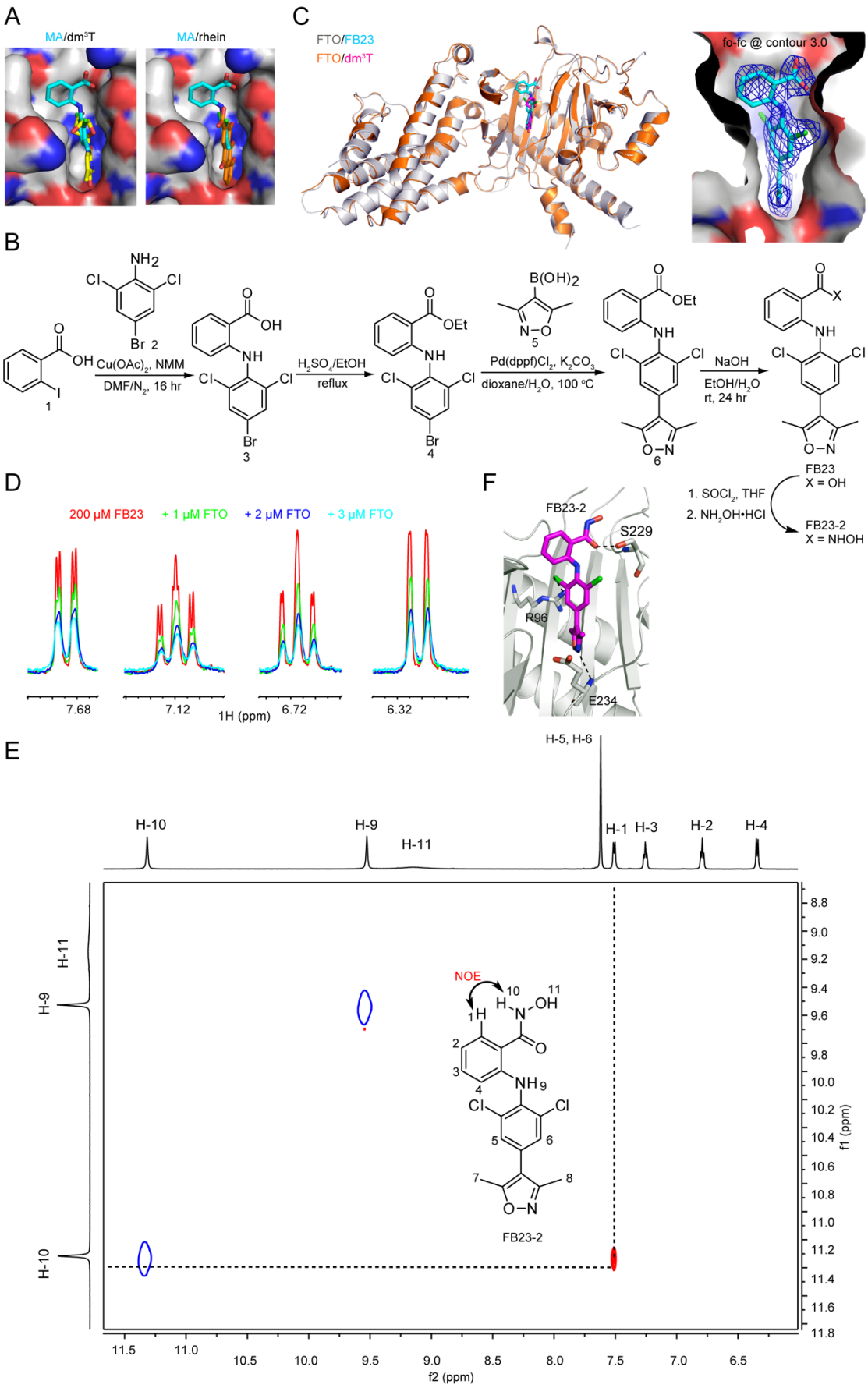
A
MA/dm³T
MA/rhein
C
FTO/FB23
FTO/dm³T
fo-fc @ contour 3.0
B
Cu(OAc)2, NMM
DMF/N2, 16 hr
H2SO4/EtOH
reflux
Pd(dppf)Cl2, K2CO3
dioxane/H2O, 100 °C
NaOH
EtOH/H2O
rt, 24 hr
1
2
3
4
5
6
FB23
X = OH
1. SOCl2, THF
2. NH2OH•HCl
FB23-2
X = NHOH
D
200 μM FB23
+ 1 μM FTO
+ 2 μM FTO
+ 3 μM FTO
7.68
7.12
6.72
6.32
1H (ppm)
F
FB23-2
S229
R96
E234
E
H-5, H-6
H-10
H-9
H-11
H-1
H-3
H-2
H-4
NOE
f2 (ppm)
f1 (ppm)

Figure S1. Development of FTO inhibitor FB23 and FB23-2, Related to Figure 1. (A) Structural complexes of FTO bound with different ligands. MA from FTO/MA complex (PDB code 4QKN) is colored in cyan, dm^3T from FTO/dm^3T complex (PDB code 3LFM) in yellow, and rhein from FTO/rhein complex (PDB code 4IE7) in orange, respectively. The structural superimpositions indicate a strategy to design a more potent inhibitor based on MA scaffold. (B) Synthetic scheme of compound FB23 and FB23-2. (C) Crystal structure of FTO bound with FB23. The overall structural complex of FTO/FB23 was colored in grey, and FB23 was colored in cyan. FTO protein in the structural complex of FTO/dm^3T was colored in orange, and dm^3T in magenta. The structural superimposition was performed in PyMol. The simulated annealing Fo-Fc density map contoured to 3.0 sigma was showed in blue color to confirm that FB23 is indeed bound. (D) NMR measurement of direct interaction between FB23 and FTO protein. NMR-CPMG spectra were recorded for FB23 at 200 μM (red), and in the presence of FTO at 1.0 μM (green), 2.0 μM (blue), and 3.0 μM (cyan), respectively. (E) ^1H nuclear Overhauser effect spectroscopy (NOESY) for FB23-2. The relative configuration of the benzohydroxamic acid in FB23-2 was interfered from the NOE correlation between H-1 and H-10 in the NOESY spectrum, which reveals a hydrogen-bond between H-9 and the carbonyl. (F) Molecular docking of FB23-2 into the structural complex of FTO/FB23. This was performed in PyMOL according to the absolute configuration of FB23-2 determined by both X-ray (see Figure 1H) and NOESY experiment.

Table S1. Data collection and refinement statistics[a], Related to Figure 1.

	FTO/FB23 (6AKW)
Data collection	
Space group	H 3
Cell dimensions	
a, *b*, *c* (Å)	141.39, 141.39, 83.61
α, β, γ (°)	90, 90, 120
Resolution (Å)	30.0-2.20 (2.28-2.20)[b]
No. of observations	224472
No. unique	31725 (3187)
R_{sym}[c]	0.067 (0.804)
$I/\sigma(I)$	27.3 (1.83)
Completeness (%)	100 (99.8)
Redundancy	7.1 (5.8)
Data refinement	
Resolution (Å)	28.74-2.20
No. reflections	27969
Completeness (%)	88.2
R_{work}/R_{free}	0.212/0.254
No. atoms	
protein	3476
ligand	35
water	153
Wilson B factors (Å^2)	29.2
Rmsd[d] in	
Bond lengths (Å)	0.002
Bond angles (º)	0.651
Ramachandran Plot	
Favored (%)	98.6
Allowed (%)	1.4

[a]The structure was solved using one crystal.

[b]Highest resolution shell is shown in parenthesis.

[c]$R_{sym} = \Sigma|(I - \langle I \rangle)|/\Sigma(I)$, where I is the observed intensity.

[d]Root mean squared deviation.

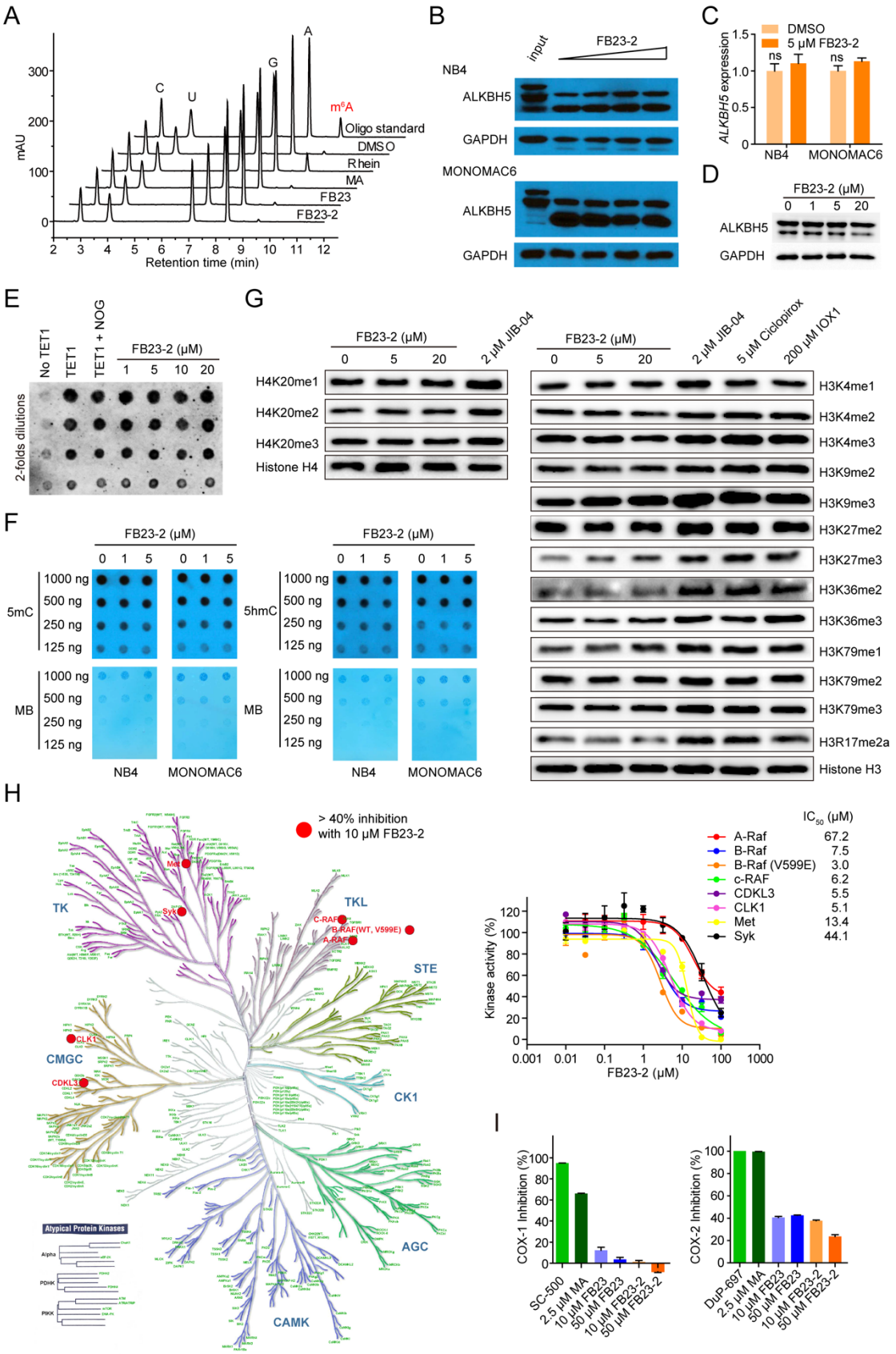

Figure S2. Selectivity profile of FTO inhibitors, Related to Figure 3. (A) Selectivity of FB23 and FB23-2 towards ALKBH5 demethylase. The ALKBH5 demethylation of m^{6}A in

RNA in the absence and presence of inhibitors was detected by HPLC. ALKBH5 is active on m^6A RNA substrate, which is observed to be inhibited by rhein at 50 μM, but not FB23 or FB23-2. (B) Representative DARTS results for ALKBH5 abundance by western blot. 50 μM, 200 μM and 500 μM FB23-2 were incubated with AML cell lysates for 1 hr at room temperature before pronase digestion. The results are derived from two biological replicates. (C) Effects of FB23-2 on *ALKBH5* expression in NB4 and MONOMAC6 AML cells analyzed by RT-qPCR. The cells were treated by DMSO or 5 μM FB23-2 for 72 hr. (D) Effects of FB23-2 on ALKBH5 abundance in NB4 AML cells detected by western blot. The cells were treated by DMSO or FB23-2 at indicated concentration for 48 hr. The results are derived from two biological replicates. (E) Effects of FB23-2 on enzymatic activity of TET1 by 5hmC dot blot. (F) Effects of FB23-2 on the abundance of global 5mC and 5hmC on DNA in NB4 and MONOMAC6 AML cells via dot blot assay. The AML cells were treated by DMSO or FB23-2 for 48 hr. MB (Methylene Blue) represents loading control of RNA samples. (G) Effects of FB23-2 on the abundance of histone methylation in NB4 AML cells by western blot. The NB4 AML cells were treated by DMSO or inhibitors as indicated for 48 hr. Representative results are derived from two biological replicates. (H) Selectivity of FB23-2 towards human kinases. The percentage inhibition of 405 human kinases by 10 μM FB23-2 was mapped onto the kinome phylogenetic tree. All the screened kinases have the names in green. Kinases inhibited more than 40% have red circles, which were further assayed for the IC_{50} calculation. Illustration reproduced courtesy of Cell Signaling Technology, Inc (www.cellsignal.com). (I) Selectivity of FB23 and FB23-2 towards COX-1 and COX-2. MA significantly inhibits COX-1 and COX-2 at 2.5 μM, while FB23 or FB23-2 minimally inhibits COX-1 and COX-2 even at 50 μM. SC-500 and DuP-697 are assayed as positive controls. These experiments were performed in duplicate.

Table S2. Inhibitions of epigenetic targets by FB23 or FB23-2, Related to Figure 3.

Epigenetic targets	Inhibition @ 10 μM (%)		Control	IC_{50} of control
	FB23	FB23-2		
HDAC1	4	13	SAHA	8.2 nM
HDAC9	2	5	TMP269	49 nM
SIRT2	11	17	Suramin	8.6 μM
BRD4(1,2)	12	38 (IC_{50} > 100 μM)	(+)-JQ-1	41 nM
DOT1L	15	11	SAH	0.84 μM
JAR1D1A	2	2	2,4-PDCA	0.45 μM
JMJD2A	-1	13	2,4-PDCA	88 nM
JMJD3	5	13	GSK-J1	0.14 μM
LSD1	14	14	RN-1	29 nM
FBXL11	-6	1	Daminozide	0.21 μM

Table S3. Enzymatic inhibition of proteases by FB23-2, Related to Figure 3.

Protease	Inhibition @ 10 μM (%)	Control	IC_{50} of control
Caspase 2	-2	Z-VDVAD-FMK	2.42 μM
Caspase 8	1	Ac-IETD-CHO	6.87 nM
Caspase 9	6	Z-LEHD-FMK	0.14 μM
Cathepsin D	0	Pepstatin A	1.26 nM
Cathepsin F	11	E-64	0.031 μM
Cathepsin H	0	E-64	0.96 μM
Cathepsin L	-2	Leupeptin	4.22 nM
Cathepsin S	11	E-64	1.75 nM
Cathepsin Z	12	Leupeptin	0.38 μM
MMP-8	5	GM-6001	0.69 nM
MMP-14	-4	GM-6001	11.7 nM
TACE	6	GM-6001	0.036 μM

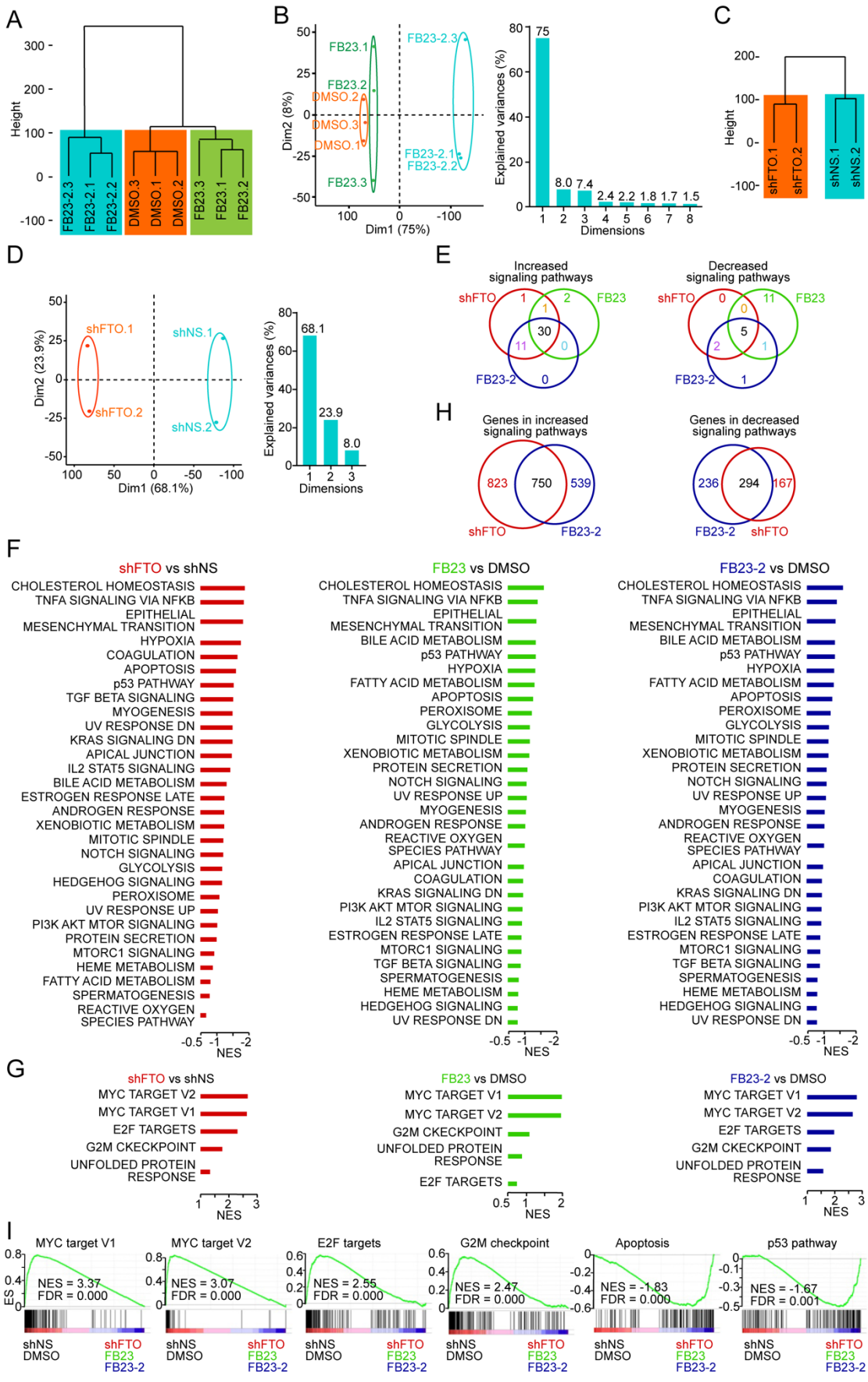
A
Height
FB23-2.3
FB23-2.1
FB23-2.2
DMSO.3
DMSO.1
DMSO.2
FB23.3
FB23.1
FB23.2
B
Dim2 (8%)
Dim1 (75%)
FB23.1
FB23.2
DMSO.2
DMSO.3
DMSO.1
FB23.3
FB23-2.3
FB23-2.1
FB23-2.2
Explained variances (%)
Dimensions
75
8.0
7.4
2.4
2.2
1.8
1.7
1.5
C
Height
shFTO.1
shFTO.2
shNS.1
shNS.2
D
Dim2 (23.9%)
Dim1 (68.1%)
shFTO.1
shFTO.2
shNS.1
shNS.2
Explained variances (%)
Dimensions
68.1
23.9
8.0
E
Increased signaling pathways
shFTO
FB23
FB23-2
1
2
1
30
11
0
0
Decreased signaling pathways
shFTO
FB23
FB23-2
0
11
0
5
2
1
1
H
Genes in increased signaling pathways
823
750
539
shFTO
FB23-2
Genes in decreased signaling pathways
236
294
167
FB23-2
shFTO
F
shFTO vs shNS
CHOLESTEROL HOMEOSTASIS
TNFA SIGNALING VIA NFKB
EPITHELIAL MESENCHYMAL TRANSITION
HYPOXIA
COAGULATION
APOPTOSIS
p53 PATHWAY
TGF BETA SIGNALING
MYOGENESIS
UV RESPONSE DN
KRAS SIGNALING DN
APICAL JUNCTION
IL2 STAT5 SIGNALING
BILE ACID METABOLISM
ESTROGEN RESPONSE LATE
ANDROGEN RESPONSE
XENOBIOTIC METABOLISM
MITOTIC SPINDLE
NOTCH SIGNALING
GLYCOLYSIS
HEDGEHOG SIGNALING
PEROXISOME
UV RESPONSE UP
PI3K AKT MTOR SIGNALING
PROTEIN SECRETION
MTORC1 SIGNALING
HEME METABOLISM
FATTY ACID METABOLISM
SPERMATOGENESIS
REACTIVE OXYGEN SPECIES PATHWAY
NES
FB23 vs DMSO
CHOLESTEROL HOMEOSTASIS
TNFA SIGNALING VIA NFKB
EPITHELIAL MESENCHYMAL TRANSITION
BILE ACID METABOLISM
p53 PATHWAY
HYPOXIA
FATTY ACID METABOLISM
APOPTOSIS
PEROXISOME
GLYCOLYSIS
MITOTIC SPINDLE
XENOBIOTIC METABOLISM
PROTEIN SECRETION
NOTCH SIGNALING
UV RESPONSE UP
MYOGENESIS
ANDROGEN RESPONSE
REACTIVE OXYGEN SPECIES PATHWAY
APICAL JUNCTION
COAGULATION
KRAS SIGNALING DN
PI3K AKT MTOR SIGNALING
IL2 STAT5 SIGNALING
ESTROGEN RESPONSE LATE
MTORC1 SIGNALING
TGF BETA SIGNALING
SPERMATOGENESIS
HEME METABOLISM
HEDGEHOG SIGNALING
UV RESPONSE DN
NES
FB23-2 vs DMSO
CHOLESTEROL HOMEOSTASIS
TNFA SIGNALING VIA NFKB
EPITHELIAL MESENCHYMAL TRANSITION
BILE ACID METABOLISM
p53 PATHWAY
HYPOXIA
FATTY ACID METABOLISM
APOPTOSIS
PEROXISOME
GLYCOLYSIS
MITOTIC SPINDLE
XENOBIOTIC METABOLISM
PROTEIN SECRETION
NOTCH SIGNALING
UV RESPONSE UP
MYOGENESIS
ANDROGEN RESPONSE
REACTIVE OXYGEN SPECIES PATHWAY
APICAL JUNCTION
COAGULATION
KRAS SIGNALING DN
PI3K AKT MTOR SIGNALING
IL2 STAT5 SIGNALING
ESTROGEN RESPONSE LATE
MTORC1 SIGNALING
TGF BETA SIGNALING
SPERMATOGENESIS
HEME METABOLISM
HEDGEHOG SIGNALING
UV RESPONSE DN
NES
G
shFTO vs shNS
MYC TARGET V2
MYC TARGET V1
E2F TARGETS
G2M CKECKPOINT
UNFOLDED PROTEIN RESPONSE
NES
FB23 vs DMSO
MYC TARGET V1
MYC TARGET V2
G2M CKECKPOINT
UNFOLDED PROTEIN RESPONSE
E2F TARGETS
NES
FB23-2 vs DMSO
MYC TARGET V1
MYC TARGET V2
E2F TARGETS
G2M CKECKPOINT
UNFOLDED PROTEIN RESPONSE
NES
I
MYC target V1
NES = 3.37
FDR = 0.000
MYC target V2
NES = 3.07
FDR = 0.000
E2F targets
NES = 2.55
FDR = 0.000
G2M checkpoint
NES = 2.47
FDR = 0.000
Apoptosis
NES = -1.83
FDR = 0.000
p53 pathway
NES = -1.67
FDR = 0.001
ES
shNS
DMSO
shFTO
FB23
FB23-2

Figure S3. Transcriptome-wide analysis of RNA-seq assays with *FTO* KD and inhibition in NB4 cells, Related to Figure 5. (A and B) Hierarchical clustering (A) and PCA (B) on FB23, FB23-2, and DMSO treated groups. The NB4 cells were exposed to DMSO or 5 μM inhibitor for 48 hr. (C and D) Hierarchical clustering (C) and PCA (D) on shFTO and shNS treated groups. shNS is the control shRNA. (E) Venn diagram of the changed signaling pathways by *FTO* KD and FTO inhibitors induced FTO inhibition. (F and G) Detailed information for the 30 co-increased pathways (F) and 5 co-decreased pathways (G) enriched in shFTO vs shNS, FB23 vs DMSO, and FB23-2 vs DMSO groups. Normalized enrichment score (NES) indicated the analysis results across gene sets. (H) Venn diagram of the genes in deregulated signaling pathways shared by *FTO* KD and FB23-2 mediated FTO inhibition. (I) GSEA analysis of increased and decreased cell proliferation, cell cycle, and cell apoptosis related pathways between (shFTO + FB23 + FB23-2) vs (shFTO + DMSO). ES represents enrichment score. False discovery rate (FDR) presented if a set was significantly enriched.

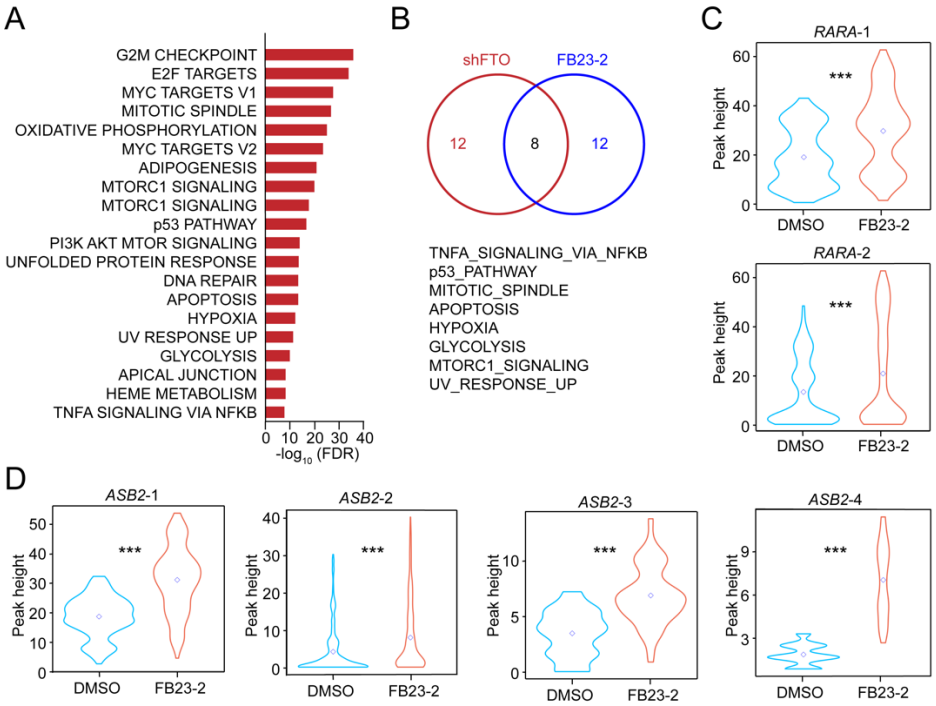

Figure S4. Analysis of m^{6}A-seq assays with *FTO* KD and FB23-2 inhibition in MONOMAC6 cells, Related to Figure 6. (A) GSEA analysis of the genes with increased m^{6}A abundance upon *FTO* KD identified by m^{6}A-seq in MONOMAC6 cells. The

MONOMAC6 cells were treated with DMSO or 5 μM FB23-2 for 72 hr. (B) Venn diagram of the co-increased and co-decreased signaling pathways by *FTO* KD and FB23-2 induced FTO inhibition. Among them, p53 and apoptosis pathways are also enriched. (C and D) The signal densities diagram of the distributions and heights of the m^{6}A peaks in *RARA* (C) and *ASB2* (D) identified by m^{6}A-seq in MONOMAC6 cells upon DMSO and 5 μM FB23-2 treatment for 72 hr. ***, $p < 0.001$.

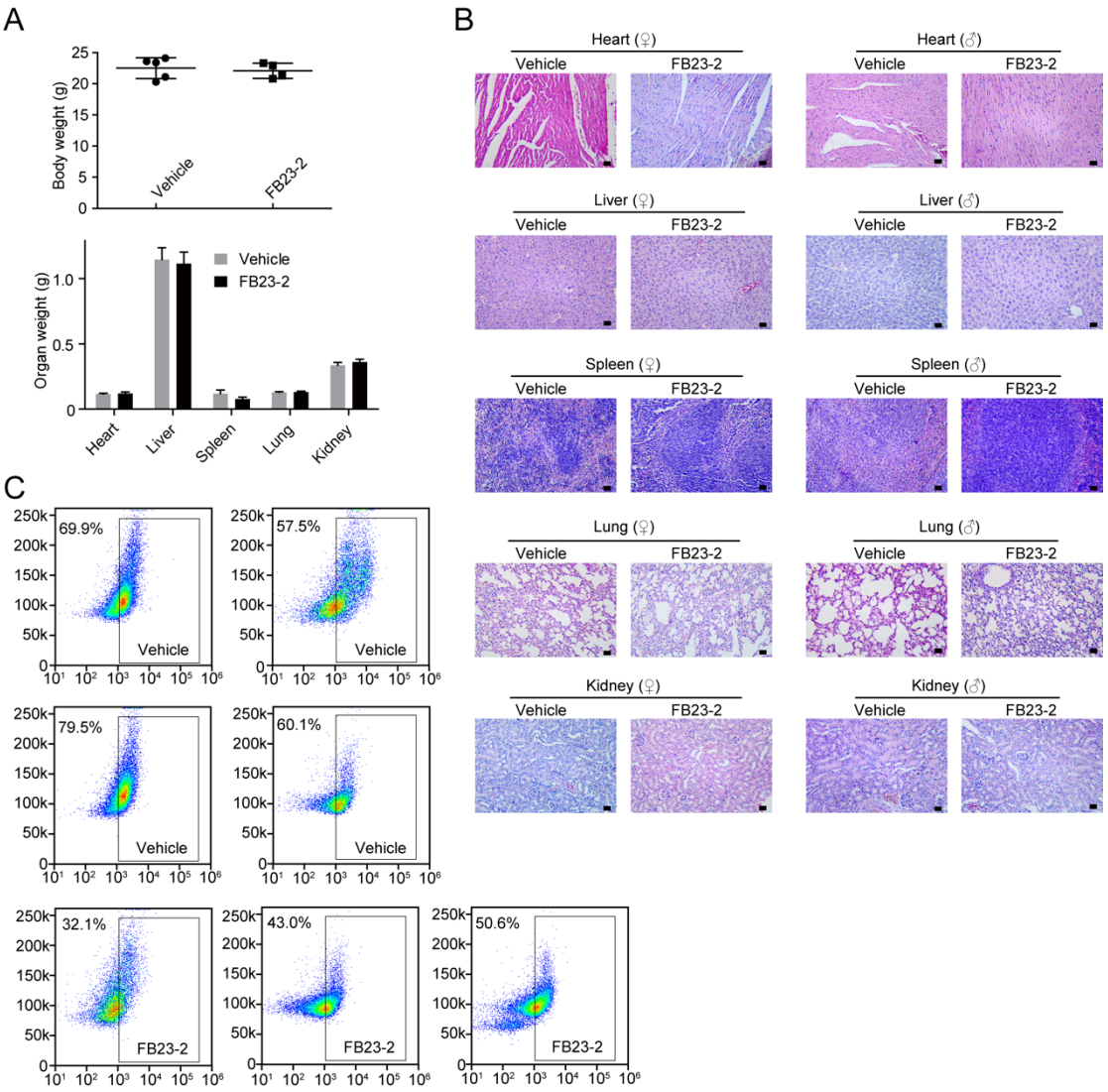

Figure S5. FB23-2 inhibition of leukemogenesis on mice, Related to Figure 7. (A) The weight of body and organs of male BALB/c mice at day 15. The mice (n = 5) were treated with vehicle or FB23-2 at a dose of 20 mg/kg daily for 14 days. (B) Histological

morphology of H&E-stained tissue sections of representative mice after treatment of 14 days with vehicle or FB23-2 at a dose of 20 mg/kg daily. Bar, 100 μm. (C) Abundance of leukemic cells into NSGS mice. The abundance of human leukemic MONOMAC6 cell into PB of recipient NSGS mice was assessed via staining human CD33. The x-axis represents hCD33-PE, and y-axis represents SSC.

Table S5. The complete blood content analysis of BALB/c mice (n = 5) treated with FB23-2 for 14 days, Related to Figure 7.

Test (unit)	Vehicle (♀) (Mean ± SD)	20 mg/kg (♀) (Mean ± SD)	Vehicle (♂) (Mean ± SD)	20 mg/kg (♂) (Mean ± SD)
WBC ($x10^9$ cells/L)	2.30 ± 0.63	3.74 ± 1.26	5.52 ± 1.44	5.94 ± 1.75
NEUT ($x10^9$ cells/L)	0.79 ± 0.13	1.83 ± 0.66	2.40 ± 1.02	3.52 ± 1.26
LYM ($x10^9$ cells/L)	1.39 ± 0.56	1.59 ± 0.73	2.87 ± 0.91	2.12 ± 0.52
MONO ($x10^9$ cells/L)	0.05 ± 0.01	0.09 ± 0.05	0.09 ± 0.03	0.14 ± 0.08
EOS ($x10^9$ cells/L)	0.07 ± 0.01	0.20 ± 0.24	0.07 ± 0.07	0.07 ± 0.08
BASO ($x10^8$ cells/L)	0.05 ± 0.03	0.06 ± 0.03	0.15 ± 0.06	0.14 ± 0.07
RBC ($x10^{12}$ cells/L)	9.69 ± 0.27	8.94 ± 0.79	9.92 ± 0.80	8.45 ± 0.92
PLT ($x10^9$ cells/L)	1201.50 ± 44.59	1288.60 ± 78.68	1461.60 ± 683.40	1449.00 ± 205.7
RET ($x10^9$ cells/L)	487.35 ± 39.17	618.62 ± 299.82	484.44 ± 221.34	549.63 ± 134.79
MCH (pg)	15.20 ± 0.14	14.96 ± 0.25	15.04 ± 0.43	15.20 ± 0.22
MCV (fL)	48.25 ± 1.06	47.60 ± 0.82	47.50 ± 0.68	48.63 ± 1.31
MCHC (g/L)	313.50 ± 4.20	314.20 ± 4.09	316.00 ± 7.68	313.00 ± 11.6
HGB (g/L)	147.25 ± 4.11	133.60 ± 11.97	149.20 ± 15.79	129.00 ± 15.64
HCT (%)	46.95 ± 0.60	42.52 ± 3.83	47.16 ± 4.22	41.05 ± 3.5
RDW (%)	13.50 ± 0.80	14.20 ± 1.22	14.10 ± 0.80	13.95 ± 0.45

Table S6. The plasma biochemistry analysis of BALB/c mice (n = 5) treated with FB23-2 for 14 days, Related to Figure 7.

Test (unit)	Vehicle (♀) (Mean ± SD)	20 mg/kg (♀) (Mean ± SD)	Vehicle (♂) (Mean ± SD)	20 mg/kg (♂) (Mean ± SD)
TBIL (μmol/L)	0.64 ± 0.77	1.50 ± 1.57	0.64 ± 0.77	0.68 ± 0.78
TP (g/L)	47.60 ± 2.20	43.3 ± 2.96	47.60 ± 2.20	50.36 ± 5.98
ALB (g/L)	26.52 ± 1.00	24.15 ± 1.59	26.52 ± 1.00	30.64 ± 5.47
GLB (g/L)	21.08 ± 1.47	19.15 ± 1.38	21.08 ± 1.47	19.72 ± 2.39
A/G	2.52 ± 0.18	2.60 ± 0.00	2.52 ± 0.18	3.12 ± 0.72
ALT (U/L)	40.80 ± 16.89	36.67 ± 11.55	40.80 ± 16.89	56.40 ± 36.56
AST (U/L)	137.2 ± 32.3	113.33 ± 30.09	137.2 ± 32.3	176.00 ± 72.94
AST/ALT	7.46 ± 2.69	5.33 ± 2.19	7.46 ± 2.69	7.29 ± 3.03
ALP (U/L)	41.20 ± 20.47	23.5 ± 25.16	41.20 ± 20.47	58.00 ± 22.72
UREA (mmol/L)	7.05 ±1.61	8.67 ± 0.85	7.05 ±1.61	10.49 ± 1.68
CR (μmol/L)	2.00 ± 0.00	2.00 ± 0.00	2.00 ± 0.00	2.00 ± 0.00
GLU (mmol/L)	2.94 ± 1.14	3.48 ± 2.36	2.94 ± 1.14	4.48 ± 1.77
TC (mmol/L)	2.63 ± 0.25	2.11 ± 0.42	2.63 ± 0.25	3.02 ± 0.69
TG (mmol/L)	1.84 ± 0.44	1.01 ± 0.27	1.84 ± 0.44	1.63 ± 0.40
CK (U/L)	615.20 ± 195.61	842.00 ± 658.18	615.20 ± 195.61	743.60 ± 330.79
K (mmol/L)	7.04 ± 0.80	29.3 ± 27.13	7.04 ± 0.80	8.14 ± 2.17
Na (mmol/L)	233.20 ± 4.15	230.00 ± 5.89	233.20 ± 4.15	236.80 ± 1.79
CL (mmol/L)	192.60 ± 5.73	183.5 ± 10.38	192.60 ± 5.73	190.60 ± 1.67
Ca (mmol/L)	2.16 ± 0.13	1.12 ± 1.10	2.16 ± 0.13	1.90 ± 0.98
P (mmol/L)	3.09 ± 0.60	2.73 ± 0.21	3.09 ± 0.60	3.24 ± 0.45

Table S7. The pharmacokinetics of rat after i.p. administration of 3 mg/kg FB23-2, Related to Figure 7.

Analyst	T_{max} (hr)	C_{max} (ng/ml)	AUC_{0-t} (hr × ng/ml)	$AUC_{0-\infty}$ (hr × ng/ml)	MRT (hr)	$t_{1/2}$ (hr)
FB23-2	0.08	2421.3 ± 90.9	2184 ± 152	2261 ± 145	4.0 ± 0.7	6.7 ± 1.3
FB23	0.4 ± 0.1	142.5 ± 26.1	2262 ± 483	3310 ± 721	N/A	N/A

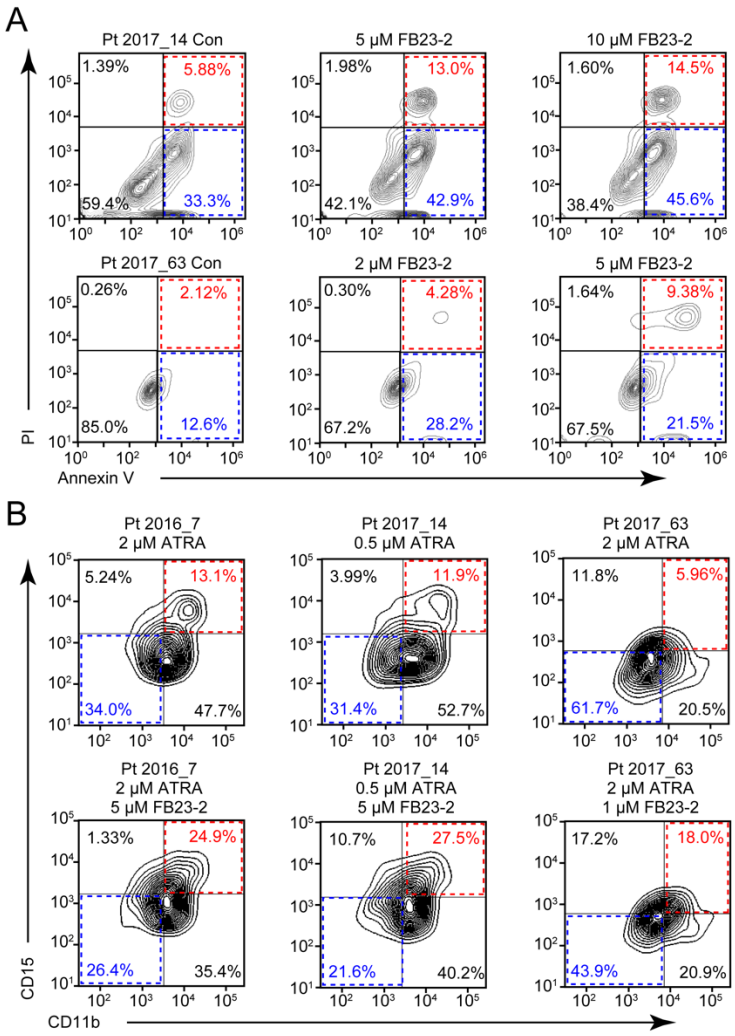

Figure S6. Effects of FB23-2 treatment on primary AML cells, Related to Figure 8. Effects of FB23-2 on cell apoptosis (A) and ATRA-induced myeloid differentiation (B) in patient AML cells analyzed by FACS. Cells for apoptosis analysis (A) were treated by DMSO or FB23-2 at indicated concentration for 48 hr, while cells for ATRA-induced myeloid analysis (B) were treated for 96 hr.

Table S8. Mutation profiles of the four primary patients. X stands for genetic alteration, Related to Figure 8.

Genetic Alterations - Gene	**Genetic Alterations - AA Alteration**	**Pt 2016_7**	**Pt 2017_14**	**Pt 2017_63**	**Pt 2014_59**
DNMT3A	R882L				X
FLT3	L576_Q577ins17				X
KRAS	G13D		X		
MLL	*MLLT3* (*AF9*) fusion	X			
MLL	*MLL-MVB12B* fusion		X		
MLL	*MLL-MLLT10* (*AF10*) fusion		X		
MNX1	t(7;12)(q36;p13) *MNX1*/*ETV6* fusion			X	
NPM1	W288fs*10+				X
PTPN11	p.D61V c.182A>T			X	
PTPN11	D61Y				X
WT1	A382fs*11, A382fs*4				X
VUS Gene	**VUS Alteration**	**Pt 2016_7**	**Pt 2017_14**	**Pt 2017_63**	**Pt 2014_59**
ASMTL	A417E	X			
ARID1A	N2220S		X		
ASXL	missense			X	
BRCA1	F486L		X		
BRCA1	N550H		X		
BRCA1	Y179C		X		
CIC	E83G	X			
DNM2	V748_S764>G	X			
EPHB1	V562I	X			
FBXO11	S747G		X		
FGFR1	R477K		X		
FLT4	V1355M		X		
GATA2	P161A		X		
HIST1H1E	A47V	X			
MAP3K1	P257L		X		
MAP3K14	G368R	X			
MET	R143Q				X
MKI67	E2658G	X			
MKI67	R116C				X
MLL	R3470H		X		

MLL3	P1863A, P1946L				X
MSH2	N596S		X		
MYC	T73H				X
NOTCH1	E1148K	X			
PIK3CG	R359H	X			
RAD21	R54L				X
STAT5B	G721S		X		
TCF3	A203T		X		
TLL2	G629A	X			
TNFRSF11A	D427N	X			
TNFRSF17	K160Q	X			
YY1AP1	G79V		X		

Table S9. Primers for RT-qPCR, Related to STAR Method.

ID	Sequence	Source
FTO-Fwd	5’-AGAATGTCTGTGACGATGTGG-3’	Generay, China
FTO-Rev	5’-GCACTTTCTGTATCGATTGCC-3’	Generay, China
ASB2-Fwd	5'-CGTGGTGCAGTTCTGTGAGT-3’	Generay, China
ASB2-Rev	5’-GTGAGCCAGAGGTCTTGGAG-3’	Generay, China
RARA-Fwd	5’-CCAGCTCCAACAGAAGCAG-3’	Generay, China
RARA-Rev	5’-AGGCCTCTGTCCAAGGAGTC-3’	Generay, China
GAPDH-Fwd	5’-GCCGCATCTTCTTTTGCGTC-3’	Generay, China
GAPDH-Rev	5’-TGAAGGGGTCATTGATGGCA-3’	Generay, China
ALKBH5-Fwd	5’-CGGCGAAGGCTACACTTACG-3’	Generay, China
ALKBH5-Rev	5’-CCACCAGCTTTTGGATCACCA-3’	Generay, China
MYC-Fwd	5’-GTCAAGAGGCGAACACACAAC-3’	Generay, China
MYC-Rev	5’-TTGGACGGACAGGATGTATGC-3’	Generay, China
CEBPA-Fwd	5’-AAGAAGTCGGTGGACAAGAACAG-3’	Generay, China
CEBPA-Rev	5’-GCGGTCATTGTCACTGGTCA-3’	Generay, China